arXiv:1401.1310v1 [cond-mat.mtrl-sci] 7 Jan 2014

Bond order potential for FeSi

P. Süle*
Research Institute for Technical Physics and Material Science,
Konkoly Thege u. 29-33, Budapest, Hungary,
sule@mfa.kfki.hu,www.mfa.kfki.hu/∼sule,

(Dated: January 8, 2014)

A new parameter set has been derived for FeSi using the Albe-Erhart-type bond order potential (BOP) and the PONTIFIX code for fitting the parameters on a large training set of various polymorphs. Ab initio calculations are also carried out to study the relative stability of various polymorphs and to use the obtained data in the training set. The original BOP formalism was unable to account for the correct energetic relationship between the B20 (ε-FeSi) and B2 (CsCl) phases and notoriusly slightly favors incorrectly the B2 polymorph. In order to correct this improper behavior the BOP potential has been extended by a Columbic term (BOP+C) in order to account for the partial ionic character of FeSi. Using this potential we are able to account for the correct phase order between the most stable B20 and B2 (CsCl) polymorphs when the net atomic charges are properly set. Although this brings in a new somewhat uncertain parameter (the net charges) one can adjust properly the BOP+C potential for specific problems. To demonstrate this we study under high pressure the B2 phase which becomes more stable vs. B20 as it is found experimentally and expected to be taken place in the Earth mantle. The obtained BOP has also been tested for the metallic and semiconducting disilicides (α-$FeSi_2$ and β-$FeSi_2$) and for the Si/β-$FeSi_2$ heterostructure. The obtained BOP, as many other BOP, overestimates the melting point (T_m) of the B20 phase by $\sim$ 1000 K if the parameters in the radial part of the potential were obtained according to the Pauling relation (regular way). Hence a special attention is paid to the T_m porblem. It has been realized that if the dimer parameters (D_0 and r_0) are adjusted irregulary (using shorter r_0 and a larger D_0 than those of the dimer), a remarkable improvement can be reached on T_m while the other properties of the potential remains nearly unaltered (except the dimer properties). We release a few sets of parameters in order to make a detailed comparative test and to demonstrate that the use of the anisotropic parameter space a significant improvement can be achieved in the melting properties with the BOP.

PACS numbers: 68.35.-p, 79.20.Rf, 81.65.Cf, 61.82.Fk, 96.35.Gt

I. INTRODUCTION

Iron-silicides have been the subject of numerous studies in various fields of Materials Science. Earth scientists consider ion-silicides as a main component of the Earth-Mantle and as such could play an important role in many processes occur in the inner region of Earth[1,2]. In particular, the stabilization of B2 (CsCl) FeSi has been studied in detail under high pressure vs. the B20 ε-FeSi at ambient conditions[48].

Computer simulations are limited to the *ab initio* density functional theory level (DFT) which does not allow the simulation of large scale systems[37]. This is because an adequate empirical potential is missing in the literature for FeSi. The main motivation of this work was to fulfill this gap.

Contrary to the importance of FeSi as a basic material, at best of our knowledge there is no reailable parameter set is available for any kind of a empirical potentials including either Buckingham-type (see e.g. ref.[7]) nor bond order-type potential functions[8] which are the basic candidates for such a binary compound. While the previous one is a simple pair potential and does not account for many-body effects, the Tersoff-Brenner formulation of bond order potentials (BOP) treat 3-body effects, e.g. bond angles adequately (angular dependence), hence a more appropriate choice for compounds with a considerable covalent characters. Unfortunately, the BOP lacks long range effects, such as Coulomb or van der Waals interactions.

Recent interesting results urge the development of a new parameter set for FeSi. These experiments on Fe-contamination driven nanopatterning on Si[50], or recent speculations on the role of FeSi plays in the Earth mantle[2], on nanowires[3] or on various interface structures[4], just to mention few examples, prove the importance of computer simulations in FeSi-related problems. Recently published results provided evidences that nanowires made from the semiconducting β-$FeSi_2$ are potentially applicable for spintronic nanodevices and exhibit photoluminescence[5]. Solar cell applications as well as the integration of nanodevices into the Si-technology could also be feasible in the near future using β-$FeSi_2$ nanowires[6].

Recent success in the development of the Albe-type bond order potentials (A-BOP)[9,10] for various materials (either in covalent, metallic or ionic nature, such as PtC[9], GaN[11], ZnO[12], GaAs, WC, SiC[13], etc.) provided evidence for the accuracy and effectiveness of the BOP formulation of empirical potentials in the prediction and reproduction of various materials properties[15,16]. The

Albe-Erhart-type BOP is based the original Brenner-formulation of BOP, however, provides more flexibility in the potential introducing further parameters. The A-type BOP can be converted into Tersoff-formalism hence any code which can handle the latter BOP can make use of A-BOP. The advantage of A-BOP is the increased flexibility of the formalism over the standard Tersoff-formalism. Moreover, the interconversion of the Tersoff-formula into the Brenner-type BOP (such as the A-BOP) is straightforward.

We use in this paper the PONTIFIX code developed for fitting the Albe-type BOP[15] for various binary compounds. The obtained new parameter set has been tested by various molecular dynamics codes (PARCAS[25], LAMMPS[26]). We find that although the new BOP for FeSi gives satisfactory results, however, the stability of the B2 phase is notoriously overestimated above the B20 phase which is the most stable form of FeSi in nature under ambient conditions. Therefore, we added a Coulombic term to the BOP in order to provide a further flexibility in the potential and physically to account for the partial ionic behaviour in this material which could stabilize the B20 phase vs. the B2 one. Similar extension of the BOP has been done recently for GaN[17]. The application of the derived new empirical potential could prove valuable, since at best of our knowledge there is no other empirical potential is available for FeSi.

II. THE GENERALIZED ALBE-ERHART-TYPE BOND ORDER POTENTIAL

We give the generalized functional form of the Albe-Erhart-type bond order potential[9,10] which includes short and long range terms,

$$E = \sum_{ij,i>j} f_{ij}(r_{ij})[V_{ij}^R - b_{ij}V_{ij}^A(r_{ij})] + E_{long}, \quad (1)$$

where for the short range repulsive and attractive pair interactions are the following, respectively,

$$V_{ij}^R = \frac{D_0}{S-1} exp(-\beta\sqrt{2S}(r-r_0)) \quad (2)$$

$$V_{ij}^A = \frac{SD_0}{S-1} exp(-\beta\sqrt{2/S}(r-r_0)) \quad (3)$$

$$b_{ij} = (1+\chi_{ij}^n)^{\frac{1}{2n}} \quad (4)$$

$$\chi = \sum_{k(\neq i,j)} f_{ik}^c(r_{ik}) g_{ik}(\Theta_{ijk}) exp[2\mu_{ik}(r_{ij}-r_{ik})] \quad (5)$$

$$g(\Theta) = \gamma \left(1 + \frac{c^2}{d^2} - \frac{c^2}{d^2 + (h + cos\Theta)^2} \right) \quad (6)$$

$$f_{ij}(r_{ij}) = \begin{cases} 1 & r \leq R_c - D_c \\ \frac{1}{2} - \frac{1}{2} sin[\frac{\pi}{2}(r-R_c)/D_c] & |r - R_c| \leq D_c \\ 0 & r \geq R_c + D_c \end{cases}$$

where R_c is the short range cutoff distance.

The long range part E_{long} has been neglected in the original formulation of the bond order formalism[9,10].

$$E_{long} = E_{Coul} + E_{Vdw} = \sum_{ij,i>j} \left[\frac{1}{4\pi\varepsilon_0} \frac{q_i q_j}{r_{ij}} + \frac{C_{Vdw}^{ij}}{r_{ij}^6} \right]_{r_{ij}<r_{cut}} \quad (7)$$

where q_i, q_j, R_c, r_{cut} and C_{Vdw}^{ij} are net atomic charges, cutoff distances and van der Waals parameter for the BOP, Coulomb and van der Waals interactions, respectively. The long range part allow us to extend the BOP for systems with partial ionic character and also one can account for long range effects excluded in the original BOP which cuts off interactions at the first neighbors.

We also study the effect of direct Coulomb interaction (BOP+C) when the Van der Waals long range part $E_{Vdw} = 0$,

$$E^{BOP+C} = \sum_{ij,i>j} f_{ij}(r_{ij})[V_{ij}^R - b_{ij}V_{ij}^A(r_{ij})]_{r_{ij}<R_c} + E_{Coul}. \quad (8)$$

The net point charges obtained from Bader's population analysis[27,28] using *ab initio* DFT calculations[22]. Instead of the diverging direct Coulomb sum in Eq. 9 the damped shift forced coulomb (DSFC) sum method[20] has been used which has been implemented by the author into the recent version of LAMMPS:

$$\frac{1}{4\pi\varepsilon_0}\frac{q_i q_j}{r_{ij}} \approx \frac{q_i q_j}{4\pi\varepsilon_0} \left(\frac{1}{r_{ij}} + \frac{r_{ij}}{r_{cut}^2} - \frac{2}{r_{cut}} \right), \quad (9)$$

where r_{cut} is the applied cutoff distance for long range interactions. The DSFC approach allows the treatment of periodic and non-periodic systems while the originally implemented Ewald and pppm approaches can be used for periodic systems only[26]. This extension of the original BOP allows us to account for the partial ionic nature present in most of the binary compounds. Although, it is rather difficult to obtain unambigously the net charges q_i. The traditionally used Mulliken charges are known to be exaggerated. It is widely accepted now that the net atomic charges obtained by the Bader's decomposition scheme (atom in molecules, AIM)[27] are more relaible and is more or less free from spurious basis set dependence. We calculate in the present paper the net charges using the SIESTA code[22] and post calculations which generate Bader's charges.

[1] The details of the interconversion can also be found in an example potential file given in the recent releases of the code LAMMPS[26]

It could be usefull to note that the obtained parameter set is compatible with the original Tersoff-formalism built in e.g. widely available MD codes, such as LAMMPS[26], we give the formulas for transforming the parameters. Note, that hereby we use the original symbols used by Tersoff[8]. The radial part of the Tersoff potential is composed of the following repulsive and attractive functions,

$$V_{ij}^R = A \times exp(-\lambda_1(r - r_0)), \tag{10}$$

$$V_{ij}^A = B \times exp(-\lambda_2(r - r_0)). \tag{11}$$

The required parameters A, B, λ_1 and λ_2 can be expressed using the Alber-Erhart parameters as follows:

$$\lambda_1 = \beta\sqrt{2S}, \lambda_2 = \beta\sqrt{2/S}, \lambda_3 = 2\mu = 0. \tag{12}$$

$$A = D_0/(S-1) * exp(\lambda_1 * r_0), \tag{13}$$
$$B = S * D_0/(S-1) * exp(\lambda_2 * r_0), \tag{14}$$

The parameters in the angular part are identical. This conversion must be done when e.g. the LAMMPS code is used. Example file can be found in the released packages of LAMMPS. Moreover, the addition of the Coulomb part to the BOP core is also straightforward using the "hybrid/overlay" option in the code LAMMPS.

III. THE PARAMETER FITTING PROCEDURE

A. The preparation of the initial guess

The selection of the initial guess for the parametrization procedure is carried out as follows: The ground state oscillation frequency of the dimer,

$$\beta = \frac{1}{2}\omega_0\sqrt{2\mu/D_0}, \tag{15}$$

where ω_0, μ and D_0 are the zero point vibration frequency, reduced mass and dissociation energy of the dimer, respectively. The values shown in Table III. have been used to calculate the initial guess β for the radial part of the BOP. The adjustment of parameter S has been done by tuning the Pauling relation for bond order (following the method proposed in recent publications[12,15]),

$$E_b = D_0 exp[-\beta\sqrt{2S}(r_b - r_0)], \tag{16}$$

where r_b is the first neighbor distance in various polymorphs, and r_0 is the dimer interatomic distance.

The obtained Pauling plot (semi-logarithmic plot) and the initial guess for the radial parameters are shown in Fig. 1. As can be seen, the fit to the DFT data results in a somewhat different curve than the one obtained by the final parametrized BOP. The reason could be that the DFT data is not fully consistent with the BOP. Unfortunatelly, experimental data is not available for the cohesive properties of the various polymorphs, hence, it is hard to consider the accuracy of the obtained DFT results. The fit of the Pauling relation given by Eq. (16) results in the fit values shown in Fig. 1. These values were used as an initial guess for the parametrization procedure.

TABLE I: The fitted parameters used in the Albe-Erhart type bond order interatomic potential for the Fe-Si interaction *The 2nd set of parameters* with the no use of Eqs (15)-(16) at the fitting prcodure. Dimer properties were allowed to be reproduced badly. No Pauling plot has been used for getting an initial guess.

Fe-Si	BOP	BOP+C
BOP-I		
D_0 (eV)	6.5588884	7.7457346
r_0 (Å)	1.5889110	1.5110803
S	1.9038691	1.6619156
β (Å^{-1})	1.0835049	1.2001554
γ	0.0809365	0.0798811
c	0.328786831	0.3327120
d	0.153064119	0.1570405
h	-0.634457610	-0.586481
R_c (Å)	2.99671618	3.097295
D_c (Å)	0.2	0.2
n	1.0	1.0
μ	1.0	1.0
BOP-II		
D_0 (eV)	3.0606066	3.1717432
r_0 (Å)	2.0493522	2.0174542
S	3.9625636	3.7495785
β (Å^{-1})	0.7292032	0.9780126
γ	0.0780215	0.0716019
c	0.3142206	0.3097108
d	0.1546207	0.1560145
h	-0.6230591	-0.8560120
R_c (Å)	3.0169527	3.1056216
BOP-IIb		
D_0 (eV)	2.4282727	2.33410201
r_0 (Å)	2.0330640	2.07023841
S	3.8251348	4.13277821
β (Å^{-1})	0.8244547	0.89583103
γ	0.068166344	0.069052916
c	0.300448478	0.30345365
d	0.159001935	0.157617464
h	-0.92396567	-1.019548197
R_c (Å)	3.170028434	3.143001937
BOP-III		
D_0 (eV)	6.4544830	5.2257579
r_0 (Å)	1.4586364	1.6094938
S	1.6830565	1.5510515
β (Å^{-1})	1.1313769	1.2645078
γ	0.076970476	0.066245953
c	0.33214478	0.30394206
d	0.15342928	0.16913177
h	-0.6523133	-0.67888934
R_c (Å)	3.02677686	3.00072535

TABLE II: The summary of the basic results obtained for the dimer FeSi. Experimental data is from ref.[29], theoretical data is taken from ref.[30].

	Expt.	Theory	BOP
BE	3.037 ± 0.259	2.236, 2.743[a], 3.217[b]	
r_0		2.19-2.23[c], 2.011-2.091[a]	
ω_0		315.6[d], 248.9[d]	

[a]* present work: DFT calculation using the molecular G03 code[51] and PBE exchange-correlation funcional or hybrid functionals such as B3LYP. [b] Obtained by the Quantum Espresso suit plane-wave DFT code (PW)[23] using the HSE functional with Hartree-Fock exchange. BE: bonding energy (eV), r_0: equilibrium distance (Å), ω_0: ground state oscillation frequency (cm^{-1}). [b] ref.[30], [c] present work: QCISD(T)/LanL2DZ, B3LYP/LanL2DZ, using G03.

TABLE III: The fitted parameters used in the bond order interatomic potential for the Fe-Si interaction transformed into the Tersoff's formula. The radial part is different only. The angular parameters are the same have shown in Table I.

Fe-Si	Tersoff	Tersoff+C
BOP-I		
A (eV)	208.785964	319.282671
B (eV)	80.664727	142.193959
λ_1 ($Å^{-1}$)	2.114289	2.18804875
λ_2 ($Å^{-1}$)	1.110522	1.31658233
BOP-II		
A (eV)	69.3743499	256.229868
B (eV)	11.8357598	18.2744415
λ_1 ($Å^{-1}$)	2.0528238	2.67824732
λ_2 ($Å^{-1}$)	0.51805447	0.714279566
BOP-IIb	lammps-bop-vi	
A (eV)	88.6557396	154.101787
B (eV)	11.0478628	11.1876165
λ_1 ($Å^{-1}$)	2.28036929	2.57550353
λ_2 ($Å^{-1}$)	0.596153974	0.623189388
BOP-III	lammps-bop-v	
A (eV)	195.135348	341.761224
B (eV)	96.1123514	148.343114
λ_1 ($Å^{-1}$)	2.07573374	2.22715079
λ_2 ($Å^{-1}$)	1.23331197	1.43589738

[a]This Table gives the parameters in those form which can be used in tersoff potential files used by e.g. LAMMPS.

In fact, we obtained two sets of parameters, BOP-I and BOP-II. The overall performance of the two force fields, as it has been shown in Table (4) is rather similar except for the melting point which used to be critical for the BOP[9]. BOP-II has been generated in a standard way hence we include this potential just for comparison and for the analysis of the results. We started from the Pauling curve in this case (BOP-II). However, we also derived another set of parameters for BOP. In this case (BOP-I) we did not stick the initial parameters to the dimer and we let the BOP to be fitted to the training set only which, however, also inlcudes the dimer.

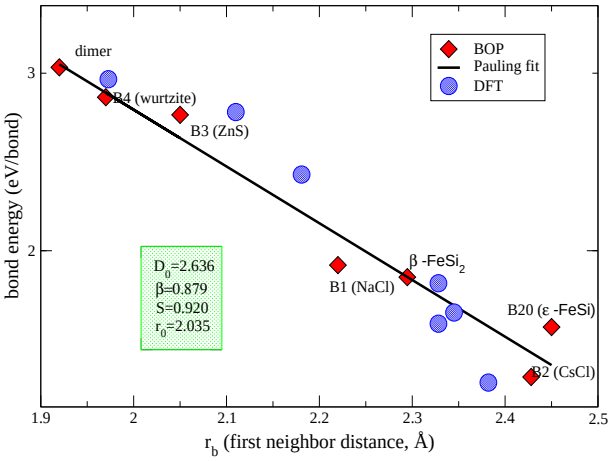

FIG. 1: Pauling plot (Eq. (16)) for BOP-II comparing data obtained from the analytic bond order potential (first parameter set) for various polymorphs. Few DFT results are also shown obtained by the author. The obtained fitted values of the Pauling bond order expression are also given. These values were used as initial guess for the radial part during the parametrization of the BOP.

[a] The Pauling bond order expression has been fitted to the DFT points shown. The obtained D_0, β and S parameters were used as initial guess for the parametrization of the BOP. r_0 has been kept fixed at $r_0 = 2.09$ Å which has been found by DFT calculations in the present work (see Table III.).

The basic difference between the two parameter fitting procedure is, however, in the following. In the case of BOP-II one can simply generate the parameters with a single iteration run with the PONTIFIX code. For BOP-I, a series of iterations have been employed recursively until a satisfactory result obtained. It turned out that this procedure moves the parameters towards larger D_0 and shorter r_0 than the equilibrium dimer values. Typically we use few tens of reiterations of intermediate parameter sets until convergence reached in the "super-iterative" fitting procedure. At the end of each iterative steps (Levenberg-Marquardt least-squares algorithm[24]) the obtained temporal parameters have been fed back to the algorythm until final convergence is reached. Hence, using a series of iterative steps instead of a single one, one can scan the parameter space for a global minimum. While BOP-II gives too large melting point ($T_m \approx 2300 \pm 100$ K), the second set gives a rather satisfactory one for the B20 phase ($T_m \approx 1550 \pm 100$ K). The overestimated melting point is a well known problem of BOP from previous publications (see. e.g. ref.[9]). This problem was mostly known for semiconductors[9]. Since this is an important issue, it could be useful to figure out while BOP-I parameter set gives much lower T_m than BOP-II. Our guess is that the initial Pauling-constraints on the initial parameter set (initial guess) put by the Pauling relation will scan those part of the complicated parameter space which prefers notorouisly the overbinding of various phases.

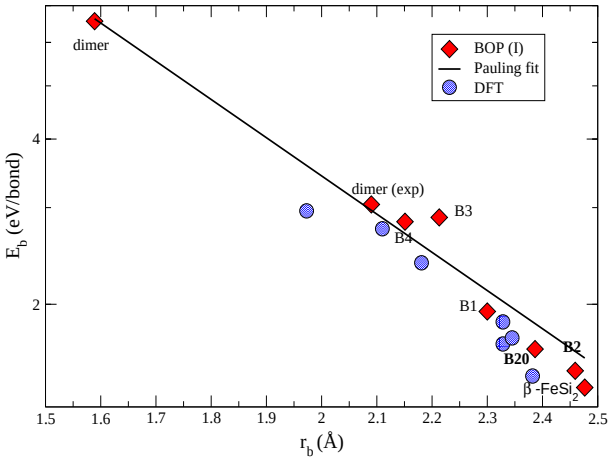

FIG. 2: The Pauling plot (Eq. (16)) for FeSi for the BOP-I parameter set comparing data obtained from the analytic bond order potential (first parameter set) for various polymorphs. Few DFT results are also shown obtained by the author. The obtained Pauling fit parameters were not used for BOP-I as initial guess and is shown here just for guiding the eye. Instead, the initial guess parameters have been obtained on a trial-and-error basis and set in manually. This way of parametrization is, however, leads to a somewhat tedious procedure with repeated samplings of the configuration space of the parameters. Typically few tens of a trials with setting in reasonable values for the radial parameters and with the recycling of the output parameters (when we find better and better values). In the case of convergence one can refine in this way the obtained parameter set.

a

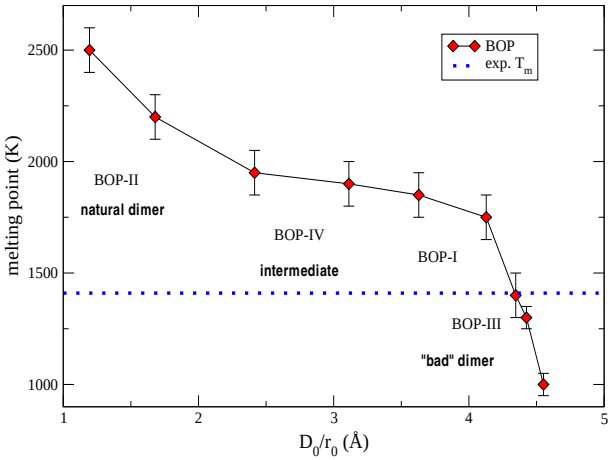

FIG. 3: The melting point against the dimer ratio D_0/r_0.

a

When this constraint is released, we allow the exploration of further "hidden" parts of the parameter space. In particular, if we allow shorter dimer equilibrium distance r_0, the BOP will provide melting at around the experimental temperature. We find that the proper melting behavior occurs when D_0 is chosen to be much higher than the experimental one together with a much shorter r_0. Hence, the selection of unphysical D_0 and r_0 leads to a more relaible BOP which performs also well for the dimer (see Fig. 2). In particular, BOP-I gives bonding energy (E_b) around the physical (experimental, $E_b \approx 3$ eV/bond) one together with a reasonable $r_b \approx 2.1$ Å (see the solid line of the Pauling fit).

B. The parametrization and the training set

The BOP potential has been parametrized using an extended training set of various structures (dimer, B1 (NaCl), B2 (CsCl), B3 (ZnS), B20 (eps-FeSi), Fe_3Si (L12a), $FeSi_3$ (L12b) phases for FeSi). The parametrization procedure has been carried out using the PONTIFIX code developed by P. Erhart and K. Albe[15,21]. For the elements similar data base has been used given by Albe and Erhart[15]. *ab initio* SIESTA[22] calculations were used to determine the cohesive energies of various structures. A Levenberg-Marquardt least-squares algorithm[24] has been implemented in Pontifix to find a combination of parameters which minimizes the deviation between the properties in the fitting database and the properties predicted by the potential. Parameter sets for different interaction types can be fitted simultaneously. The fitting database encompassed the bond lengths and energies of various structures as well as elastic constants. Subsequent fitting trials and refinements are exploited (time to time on a trial and error basis) until a satisfactory parameter set has been obtained for the most stable B20 phase. The long-range terms have also been implemented in the modified version of the PONTIFIX code which allows the explicit parametrization of the generalized BOP. Results will be shown for the BOP and BOP+C parameter sets. The parameter sets have been tested for the various polymorhps of FeSi (B1, B2, B3, B20, $\beta - FeSi_2$, $\gamma - FeSi_2$) using the modified version of the PARCAS code[25] and the LAMMPS code[26]. The DSCF method has also been implemented in the LAMMPS as well as in the PONTIFIX codes. The main advantage of the DSCF approach beyond its simplicity is that it can also be used for non-periodic systems.

C. Multiple set of parameters for various application fields

We realized that instead of developing only a universal potential with a relatively weak accuracy it is better to develop a few sets of parameters which optimized to different properties of the training set. In particular, it is hard to achieve the dimer properties accurately together with the solid state. It turned out that keeping the radial part accurately fitted to the dimer (as it has been proposed for the parametrization of the Alber-Erhart-type BOP) leads to the serious overestimation of the melting point while other properties remain acceptable.

Since in the case of FeSi it is important to simulate accurately T_m due to special application fields related to this quantity (high pressure phases of FeSi and melting see e.g. ref.[37]). Keeping this in mind we release in this paper few sets which were parametrized independently:
BOP-I: The cohesive energies are fitted to the *ab initio* training set with short r_0 and large D_0 ($r_0 \ll 2.0$ Å, $D_0 \gg 3.0$ eV) using scaled down *ab initio* DFT cohesive energies. Poor dimer property, good melting point and lattice constant, acceptable elastic properties, proper phase order of the B20 and B2 polymorphs for the BOP+C variant. The improvement of T_m is also significant for the BOP+C variant over the BOP.
BOP-II: Fitted to the ab initio training set (BOP-IIa) or to experimental heat of formation (BOP-IIb) with natural r_0 and D_0. ($r_0 \approx 2.1 \pm 0.1$ Å, $D_0 \approx 3.0 \pm 0.5$ eV). This potential provides too large melting point of $T_m > 2200$ K instead of the experimental $T_{m,exp} \approx 1450 \pm 50$ K. T_m remains high for BOP-IIb, although the cohesive energies are lowered significantly as for BOP-III. It can be taken for granted that good dimer properties keeps T_m too high. There seems to be no solution for this paradoxon. The overall performance is the following: Good at the dimer, overestimated cohesive energies (BOP-IIa), acceptable elastic properties. Bad phase order in sign for B20 vs. B1 polymorphs ($\Delta H_{B20-B2} \approx 0.15$ eV/atom instead of $\Delta H_{B20-B2,exp} \approx -0.25$ eV/atom)[46]. We do not reccomend this parameter set for applications and we include it just for demonstrative purpose.
BOP-III: Fitted to experimental heat of formation (ΔH) with short r_0 and large D_0 ($\Delta H \approx 0.5 \pm 0.2$ eV/atom) in such a way that the ab initio cohesive energies are scaled down by ~ 0.95 eV/atom in order to reproduce experimental ΔH[47]. BOP-III is not recommended for the dimer (bad dimer regime). Melting occurs at somewhat low temperature of $T_m \approx 1250 \pm 50$ K, although it is not far from $T_{m,exp} \approx 1410$ K. Cohesive energies and ΔH are realistic as being fitted to them. Phase order for B20 vs. B1 polymorphs is also in the right side ($\Delta H_{B20-B2} \approx -0.05$ eV/atom). The improvement of ΔH_{B20-B2} is also remarkable for the BOP+C variant ($\Delta H_{B20-B2} \approx -0.13$ eV/atom). As an overall conclusion we find that BOP-III performs rather well and is suitable for various application fields related to FeSi.
BOP-IV: Search for middle range parameters ($1.7 < r_0 < 2.0$ Å, $D_0 > 3.0$ eV). The combination of properties produced by BOP-I, BOP-II and BOP-III. This leads to intermediate values for r_0 and D_0. ΔH also becomes larger than the upper limit of the measured values. Unfortunatelly, it has been found that in this parameter regime T_m remains still too high at around $T_m \approx 2000 \pm 100$ K. This parameter regime proved to be unsuccessfull, hence, we do not show results in the rest of the paper.

Morever, each set is released with BOP and BOP+C variants. Theferfore, finally we end up with 8 parameter sets. One might think it is more than reasonable, however, we argue that this "zoo" of force fields make it possible to select the most appropriate one for the problem to be studied. One has to keep in mind that empirical force fields are not unique and the parameter space contains unexplored optimal regions which could be similar to each other in performance.

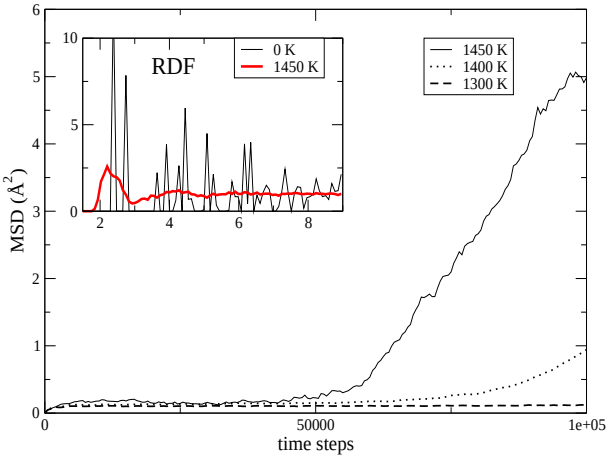

FIG. 4: The mean square of displacements (MSD) vs. time steps for the B20 system using the BOP-III+C parameter set at various temperatures. *Inset*: The radial density function (RDF) is also shown for 0 K and at around the melting point.

a

D. ab initio DFT results for the polymorphs

Since the availability of experimental results for the cohesive properties of FeSi is rather limited we calculated the cohesive energy (binding energy per atom) of various polymorphs using the SIESTA code[22]. The unit cells were optimized by the variable cell approach using standard DZP basis for Fe and an optimized TZP quality basis for Si together with standard pseudopotentials available from the homepage of SIESTA. 3×3 Monkhorst k-grid has been used. The obtained results are summarized in Table IV.

One has to keep in mind, however, that the *ab initio* DFT cohesive energies might be exagerated, which is due to the notorious overbinding behavior of LDA and GGA exchange-correlation functionals[49]. Therefore, we correct the obtained E_c^{DFT} values by $\Delta E_c \approx \Delta H_{exp}$. One can estimate the "experimental" E_c of the B20 phase using the measured formation energy of ε-FeSi, which is in the range of $\mid \Delta H_{exp} \mid \approx 0.2 - 0.65$ eV/atom[47]: $E_{c,est} \approx (\Delta H_{exp} + E_{c,Fe} + E_{c,Si})/2 \approx 4.995$ eV/atom, where $E_{c,Fe} = -4.28$ eV/atom and $E_{c,Si} = -4.63$ eV/atom are the measured cohesive energies of the constituents, respectively. We find than that the DFT GGA model overestimates the cohesive energy by some $\Delta E_c \approx \mid E_c^{DFT} - E_{c,est} \mid \approx 5.928 - 4.995 = 0.933$ eV/atom.

ΔE_c is used than to correct the *ab initio* DFT cohesive energies for fitting purpose. Hence in the fitting data base we decreased the E_c^{DFT} values by ΔE_c.

IV. RESULTS

A. Melting properties

The melting simulations have been run under NPT conditions until 1 ns using Nose-Hoover thermostat (and prestostat) as implemented in the LAMMPS code[25]. The mean square of atomic displacements and the rdf file have been analysed and compared together with the visual inspection of movie (animation) files which provide sufficient information on melting. The sharp melting transition can be seen in Fig. 3 together with the radical change in the rdf (Inset Fig. 4).

As mentioned earlier, each variants of BOP-II give rather large melting point of $T_m \approx 2500 \pm 100$ K which is attributed to the overbinding of the potential at short interatomic distances. This is the typical consequence of the $D_0/r_0 < 3.0$ ratio. Using BOP-I T_m has been lowered effectively, especially with the BOP+C variant which gives T_m nearly in perfect agreement with experiment. BOP-III underestimates T_m by 150 K due to the too large D_0/r_0 ratio.

In order to get more insight into the adjustment of T_m we have studied the variation of it as a function of the dimer parameters D_0 and r_0. In Fig. 3 one see that T_m is nearly not sensitive to D_0/r_0 within the regime of natural values ($D_0 < 4$ eV/atom, $r_0 > 1.8$ Å) and remains at around $T_m \approx 2200 \pm 200$ K. However, when $D_0/r_0 > 4.0$ T_m starts to drop. This is not surprising, if we consider that in this way we introduce a structural anisotropy into the system. The BOP tries to shorten first neighbor distances to the unphysical $r_0 < 1.6$ Å, which is hindered, however, by the repulsive potential in the solid environment put by the first neighbors on a central atom. The reason of the sensitivity of T_m to D_0/r_0 is somewhat unclear. Nevertheless, the stress what is put by the short r_0 which tries to shorten the first neighbor distances reduces T_m effectively when compared with BOP-II with natural dimer properties ($r_0 \approx 2.1$ Å, $D_0 \approx 3.0$ eV/atom). Since in the solid state the first neighbor distance can not be shorten seriously due to the strong repulsion of the first neighbors the lattice constant remains nearly unaffected to those cases where $D_0/r_0 < 3.0$ (natural dimer regime). Hence, introducing an artificial anisotropy into the radial parameter set pushes T_m in the right direction. Using then an appropriately chosen $D_0; r_0$ pair one can tune T_m effectively. The price what we pay is that the dimer is incorrectly described with this parameter set. However, our aim is to develop a BOP which describes correctly solid state with various polymorphs and not molecules. Hence, the drop of the constraint put by the Pauling relation on the initial guess parameters could lead to more effective BOP force fields in the soild state. At least the overall performance of the BOP-III set as it has been shown in Table (II) does not show serious change in the test results.

B. Phase order problem: BOP+C

BOP fails to reproduce correctly the energetic relationship (phase order) between the two most stable polymorphs (B20 and B2) of FeSi and the B2 phase is more stable by ~ 0.1 eV (see Table 3). Table 2 reports us that ab initio calculations slightly favors B20 over B2, and the energetic difference is rather small, less than 0.01 eV, which is within the accuracy of present day exchange-correlation functionals for cohesive energy. Although the difference is not negligible between the phases, one can conclude that it should be accounted for by any reliable approach (empirical, or ab initio). Therefore we decided to improve the performance of the BOP emprirical potential by adding a simple Coulomb term to it as it has been shown in Eq (9).

However, it is rather difficult to give reliable net atomic charges q_i required by the Coulomb term. As it is well known Mulliken charges are exaggerated. Instead we use Bader charges based on the atom in molecule framework[27]. The obtained partial charges for Si and Fe (± 0.15) both in B20 and B2 FeSi are shown in Table II. The net charges are calculated using the self-consistent density files obtained by SIESTA[22]. Note that the net Mulliken charges and those obtained by the Bader's are rather different. The Mulliken's approach provides larger net charges in B20 while Bader estimates smaller q in B20. What is for sure that the Mulliken charges are too large, however, it is far not trivial whether the Bader AIM charges are in the correct order. One has to keep in mind that the decomposition of the space in the system could result in small variations in the magnitude of q which could reverse the order of the charges system by system. Hence we take with some caution the obtained charges, especially their relationship to each other.

Therefore, in this way, we get still the B2 phase more stable since SIESTA provided somewhat larger q for B2. We also observe, however, that the relative stability of B2 FeSi is lost when the net charges are slightly increased to ± 0.23 in the B20 phase. Also, the net difference of $\Delta q < 0.05$ between the net charges of the B2 and B20 phases (e.g. $q_{B2} \approx 0.21$ and $q_{B20} \approx 0.25$) will slightly stabilize the B20 phase by 0.015 eV/atom. In other words, the problem is slightly sensitive to the choice of q_i. Unfortunately the choice of the appropriate q_i is somewhat arbitrary, since the obtained Bader charges seems to be understimated while the Mulliken charges are overtestimated. We find in other compounds, such as ZnO e.g., that somewhat a larger point charge is required than provided by SIESTA by $\sim 10 - 20\%$ to obtain consistent properties with experimental and ab initio ones using e.g.

TABLE IV: ab initio results for various polymorphs of FeSi (spinpolarized PBE) obtained for cohesive energy E_{cohes} (eV/atom), equilibrium lattice constant (a_{latt}) and net atomic charges/Si atom (Mulliken charges $q_{Si,M}$ and Bader's charges using the Voronoi analysis, $q_{Si,B}$).

polymorph	symbol	E_{cohes} (eV)[a]	a_{latt} (Å)	$q_{Si,M}$	$q_{Si,B}$
dimer [b]		-2.668	2.106	-0.24	-0.180
dimer [c]		-2.745	2.11	-0.273	
dimer [d]			2.00	-0.24	
B20	ε-FeSi	-5.928 (-8.370)	4.467	-0.563	-0.15
B2	CsCl	-5.920 (-7.415)	2.751	-0.338	-0.231
B1	NaCl	-5.181	4.950	-0.705	-0.134
B3	ZnS ?	-5.918	2.758	-0.344	
Fe_{3Si},	L12a	-5.991	3.595	-0.923	-0.359
Fe_{3Si}	DO3, $AlFe_3$	-3.580	4.412	-0.153	
$FeSi_3$	L12b,$CuAu_3$	-4.745	3.635	-0.120	-0.09
γ-$FeSi_2$	C1, CaF_2	-3.062	5.3	-0.295	
β-$FeSi_2$	oC48	-5.571	9.816, 7.745, 7.813		

The cohesive energy of Fe_nSi_m is $E_{cohes} = \frac{1}{n+m}\left(E_{tot}^{n,m} - nE_{Fe} - mE_{Si}\right)$, where $E_{tot}^{n,m}$ is the calculated total energy of the Fe_nSi_m system and E_{Fe} and E_{Si} are the corresponding single atomic energies.
Obtained by the fully periodic code SIESTA[22]. The results obtained by the fully periodic SIESTA code using spinpolarized and spin-unpolarized DFT calculations with the PBE xc-functional using 3×3 Monkhorst k-grid and TZTPF long basis, optimized for bulk Si[40] and a standard built-in DZP basis set for Fe. We also give cohesive energies for the B2 and B20 polymorphs in parentheses obtained by the fully periodic plane-wave QUANTUM ESPRESSO code[23] using the HSE functional with Hartree-Fock exchange (3×3 Monkhorst k-grid, 55 Ry plane wave cutoff, spin restricted).
Obtained using the molecular code Gaussian (G03)[51] using PBE/6-311G(d) xc-functional and basis set.
Also with G03 using UB3LYP/6-311G(d).
[33], Net atomic charges obtained by the Mulliken analysis (SIESTA, G03) and by natural population analysis built in G03.
[a]
[b]
*
*
*
*
*

Buckingham and Coulomb potential.

Moreover, the charge distribution as being nonlocal, the point charge model can only be relaible if the net charge is properly adjusted. There is no standard way of setting in point charges in Coulombic models and often it can be done only on a trial and error basis. We also find that the choice of $q \approx 0.25e$ in B20 FeSi and $q \approx 0.15e$ in the B2 phase gives satisfactory results. In this way the B20 polymorph becomes slightly more stable. Hence the proper choice of the net charges around the value obtained by *ab initio* calculations could account for the required stability relationship between the various polymorphs. Nevertheless, it would be fruitfull to look for a more adequate physical modell which can capture the main essence of the polymorphs without the adjustment of net charges. A possible choice could be the fitting of the COMB modell to FeSi[52]. This modell is based on the Tersoff BOP modell, and the long range part should only be adjusted. This definitly goes beyond the scope of the present paper.

[2] Unpublished results (2011)

C. Results on the B20 → B2 phase transformation

D. Results on disilicides

Iron disilicide exists in two stable modifications, the room temperature phase β-$FeSi_2$ which is orthorhombic and the high temperature phase α-FeSi2 which is tetragonal. Both phases show very interesting properties for potential applications in thermoelectrics, photovoltaics and optoelectronics[44].

E. Si-β-$FeSi_2$ heterostructures: simulated annealing

V. ACKNOWLEDGEMENT

The kind help of P. Erhart (Darmstadt) is greatly acknowledged. We wish to thank to K. Nordlund (Helsinki) for helpful discussions and constant help in the use of the PARCAS code and to S. Plimpton (Sandia) in the use of the LAMMPS code. The calculations (simulations) have been done mostly on the supercomputers of the NIIF center (Budapest). The help of the staff is also greatly

TABLE V: The comparison of BOP-I and BOP-II force fields with each other and with density functional (DFT) and experimental results for the B20 (ε-FeSi) and B2 (CsCl) polymorphs. In both cases the short-range only (BOP) and the short+long range BOPs (BOP+C) are compared. BOP-I corresponds to the parameter sets obtained for the "bad-dimer" case. BOP-II has been determined by using the standard Pauling process for fitting the radial part.

	dim	BOP-I	BOP-I+C	BOP-II	BOP-II+C	DFT	EXP	
B20 (ε-FeSi)								
a_{latt}	Å	4.465	4.468	4.490	4.491	4.75	4.489[a]	
V	Å^3							90.19
E_{cohes}	eV/atom	-4.933	-4.892	-4.841	-4.747	-5.928	-4.995 (est)	
$\|\Delta H\|$	eV/atom	0.239	0.219			0.687	0.28-0.64[b]	
γ	eV/atom	0.54	0.53	0.54	0.54	n.a.	n.a.	
T_{melt}	K	1650 ± 50	1600 ± 50	2800 ± 100	> 2000	n/a	1410[b], 1473[c]	
B	GPa	193.4	232.7	224.9	232.7	180	160-209[c]	
c_{11}	GPa	281.1	346.5	296.8	316.1	488[d]	316.7[e], 346.3[f]	
c_{12}	GPa	149.6	175.8	178.1	182.8	213	112.9, 139.2	
c_{44}	GPa	90.2	82.9	106.7	112.2	125	125.2, 105.8	
B2 (CsCl)								
	a_{latt} (Å)	2.801	2.803	2.798	2.801	2.751	2.83	
E_{cohes}	eV	-5.006	-4.906	-4.999	-4.902	-5.92	n/a	
T_{melt}	K	1850 ± 50	1800 ± 50	3000 ± 100	3200 ± 100	n/a	1650[g]	
B	GPa	257.4	267.0			223-226[h]	222[i]	
c_{11}	GPa	513.1	399.2	513.6	537.2		420[i], 364.0[j]	
c_{12}	GPa	129.5	201.0	125.5	129.9		210, 92.0	
c_{44}	GPa	43.3	73.7	45.1	52.0		95, 80.0	
ΔH_{B20-B2}	eV/atom	0.128	-0.13				~ -0.25[k]	

denotes data which is not available from the literature or we could not derive by DFT calculations (e.g. T_m), DFT results obtained in the present work using the SIESTA package[22]. Details of the calculations are given in Table III. The net charges on Si: $n_q = -0.25e$ and $n_q = -0.21e$ for the B20 and B2 polymorphs, respectively. The formation energy of Fe_nSi_m is $\Delta H = \frac{1}{n+m}\left(E_{tot}^{n,m} - nE_{c,Fe} - mE_{c,Si}\right)$, where $E_{tot}^{n,m}$ is the calculated total free energy of the Fe_nSi_m system and $E_{c,Fe} = -5.933$ and $E_{c,Si} = -4.5495$ are the corresponding atomic cohesive energies in their bcc and diamond phases as obtained by the spinpolarized PBE DFT calculations. If we take the mean experimental $\Delta H \approx 0.5$ eV/atom, hence the estimated ("experimental") cohesive energy per atom of the B20 phase is $E_c \approx (2 \times 0.5 - 4.63 - 4.28)/2 = -4.995$ eV/atom for FeSi. The experimental cohesive energies of Si (-4.63) and Fe (-4.28) have been used, respectively. ΔH_{B20-B2}: the enthalpy difference in eV/atom between the B20 and B2 phases at ambient conditions[46], γ is the surface energy (eV/atom), $\gamma = E_{c,s} - E_{c,b}$, where $E_{c,s}$ and $E_{c,b}$ are the average cohesive energy on the surface and in the bulk, respectively. [b]: The experimental heat of formation is taken from ref.[47], [c]: A different melting temperature is given in ref.[2], [e] refs.[38], [f] ref.[43], [g]48, [h]: refs.[33] and[37], [i], [j], [k] ref.[46], [m]: For B2 FeSi $n_q = -0.1e$,

*

appreciated, mostly the constant help of P. Stefan.

* Electronic address: sule@mfa.kfki.hu

[1] R. Boehler, Nature **363**, 534. (1993), R. Bastian Georg, A. N. Halliday, E. A. Schauble, B. C. Reynolds, Nature **447**, 1102 (2007).

[2] H. Asanuma, E. Ohtani, T. Sakai, H. Terasaki, S. Kamada, T. Kondo, T. Kikegawa, Phys. Chem. Minerals **37**, 353. (2010), R. Nomura, H. Ozawa, S. Tateno, K. Hirose, J. Hernlund, S. Muto, H. Ishii, Nature, **473**, 199. (2011), L. Vočadlo, Earth and Planetary Sci. Lett., **254** 227. (2007).

[3] A. L. Schmitt, M. J. Bierman, D. Schmeisser, F. J. Himpsel, and Song Jin, Nano Lett. **6**, 1617 (2006), K. Seo, N. Bagkar, S. Kim, J. In, H. Yoon, Y. Jo, B. Kim, Nano Lett. **10**, 3643. (2010),

[4] S. Walter , F. Blobner , M. Krause , S. Muller , K. Heinz

TABLE VI: The summary of the basic results obtained by various long range electrostatics for the B20 and B2 polymorphs of FeSi using the BOP-III+C force field.

B20	Coulomb	E_{cohes} (eV)	a_{latt} (Å)	T_{melt} (K)	B (GPa)
BOP+C	DSFC	-4.913	4.468	1400 ± 50	227
	Ewald	-4.902	4.465	1200 ± 50	n/a
	PPPM	-4.902	4.465	1200 ± 50	n/a
	Wolf	-4.782	4.487		n/a
Exp			4.49	1450 ± 50	¡209
B2					
BOP+C	DSFC	-5.007	2.802	1200 ± 50	
	Ewald	-4.885	2.800	1100 ± 50	
	PPPM	-4.899	2.801	n/a	
Exp			2.83	1650 ± 50	222

[a] The net charges of $q = \pm 0.15$ have been used for the B2 and B20 phases. DSFC: damped shift forced coulomb[20], Ewald-sum, PPPM: Particle-Particle Particle-Mesh using an iterative Poisson solver (details are given in the corresponding LAMMPS manual). The long range cutoff distance is $r_{cut} = 12.0$ Å. Wolf: Wolf's summation method[32] as implementes in LAMMPS.

and U. Starke, J. Phys.: Condens. Matter **15** 5207. (2003).

[5] S-W. Hung, P-H. Yeh, L-W. Chu, C-D. Chen, L-J. Chou, Y-J. Wu and L.-J. Chen, J. Mater. Chem., **21**, 5704. (2011).

[6] A. S. W. Wong, G. W. Ho, S. L. Liew, K. C. Chua1 and D. Z. Chi, Prog. Photovolt: Res. Appl. **19**, 464. (2011).

[7] J. D. Gale, Phil. Mag. **B73**, 3 (1996).

[8] J. Tersoff, Phys. Rev. Lett. 56, 632 (1986), Phys. Rev. **B37**, 6991. (1988), Phys. Rev. Lett. **61**, 2879. (1988), Phys. Rev. **B39**, 5566. (1989), D.W. Brenner, Phys. Rev. **B42**, 9458.(1990), Brenner, D. W., Phys. Rev. Lett. **63**, 1022. (1989).

[9] Albe, K., K. Nordlund, J. Nord, and A. Kuronen, Phys. Rev. **B66**, 035205. (2002), Albe, K. A., K. Nordlund, and R. S. Averback, Phys. Rev. **B65**, 195124. (2002).

[10] Nord, J., K. Albe, P. Erhart, and K. Nordlund, 2003, J. Phys.: Condens. Matter **15**, 5649. (2003).

[11] J. Nord , K. Albe , P. Erhart and K. Nordlund, J. Phys.: Condens. Matter **15** 5649 (2003).

[12] P. Erhart, N. Juslin, O. Goy, K. Nordlund, R. Muller, J. Phys.: Condens. Matter **18** 6585 (2006).

[13] P. Erhart and K. Albe, Phys. Rev. **B71**, 035211 (2005).

[14]

[15] M. Müller, P. Erhart and K. Albe, J. Phys.: Condens. Matter **19**, 326220 (2007), P. Erhart and K. Albe, Phys. Rev. **B71**, 035211 (2005).

[16] P. Süle, J. Chem. Phys.**134**, 244706 (2011).

[17] K. Albe, J. Nordb and K. Nordlund, Phil. Mag., **89**, 3477. (2009).
Geophys. Res. Lett., **37** L02305 (2010).

[18] Miglio L., Tavazza F. and Malegori G., Appl. Phys. Lett., **67**, (1995) 2293.

[19] M. Fanciulli, G. Weyer, J. Chevallier, H. von Kanel, H. Deller, N. Onda, L. Miglio, F. Tavazza and M. Celino, Europhys. Lett., **37**, 139. (1997).

[20] C. Fennel, Z. Gezelter, J. Chem. Phys., **124**, 234104 (2006)

[21] P. Erhart, K. Albe, Pontifix/Pinguin: *A Program Package for Fitting Interatomic Potentials of the Bond-Order*, http://www.mm.mw.tu-darmstadt.de/pontifix

[22] E. Artacho, E. Anglada, O. Dieguez, J. D. Gale, A. Garca, J. Junquera, R. M. Martin, P. Ordejn, J. M. Pruneda, D. Snchez-Portal and J. M. Soler, J. Phys.: Condens. Matter **20**, 064208 (2008).

[23] P. Giannozzi, S. Baroni, N. Bonini, M. Calandra, R. Car, C. Cavazzoni, D. Ceresoli, G. L. Chiarotti, M. Cococcioni, I. Dabo, A. Dal Corso, S. Fabris, G. Fratesi, S. de Gironcoli, R. Gebauer, U. Gerstmann, C. Gougoussis, A. Kokalj, M. Lazzeri, L. Martin-Samos, N. Marzari, F. Mauri, R. Mazzarello, S. Paolini, A. Pasquarello, L. Paulatto, C. Sbraccia, S. Scandolo, G. Sclauzero, A. P. Seitsonen, A. Smogunov, P. Umari, R. M. Wentzcovitch, J. Phys. Condens. Matter **21**, 395502 (2009).

[24] Press, W. H., S. A. Teukolsky, W. T. Vetterling, and B. P. Flannery, 1995, Numerical Recipes in Fortran 77: The Art of Scientific Computing (Cambridge University Press, New York), chapter 11, 2nd edition.

[25] K. Nordlund, Comput. Mater. Sci, **3**, 448. (1995), K. Nordlund, *et al.*, Phys. Rev., **B57** 7556. (1998), P. Süle, modified PARCAS (2008-2010).

[26] S. J. Plimpton, *Fast Parallel Algorithms for Short-Range Molecular Dynamics*, J. Comp. Phys., **117**, 1-19 (1995).

[27] G. Henkelman, A. Arnaldsson, and H. Jonsson Comput. Mater. Sci. **36**, 254-360 (2006).

[28] R. F. W. Bader, *Atoms in Molecules - A Quantum Theory*, Oxford University Press, Oxford, (1990).

[29] A. Vander Auwera-Mahieu, N. S. McIntyre and J. Drowart Chem. Phys. Lett., **4**, 198 (1969).

[30] Z. J. Wu and Z. M. Su, J. Chem. Phys. **124**, 184306. (2006), W. Huang, C. E. Zybill, L. L., W. Hieringer, and H. H. Huang, Organomet., **17**, 5825 (1998).

[31] A. I. Al-Sharif, M. Abu-Jafar, and A Qteish., J. Phys.: Condens. Matter **13** 2807 (2001).

[32] D. Wolf, P. Keblinski, S. R. Phillpot, J. Eggebrecht, J. Chem Phys, **110**, 8254 (1999).

[33] E. G. Moroni, W. Wolf, J. Hafner, R. Podloucky, Phys. Rev. **B59**, 12860. (1999).

[34] G. Profeta, S. Picozzi, and A. Continenza, Phys. Rev. **B70**, 235338 (2004)

[35] S. Walter, F. Blobner, M. Krause, S. Muller, K. Heinz and U. Starke, J. Phys.: Condens. Matter **15** 5207. (2003).

[36] V. Milekhinea, M.I. Onsoienb, J.K. Solberga, T. Skalandc, Intermetallics **10**, 743 (2002).

[37] L. Vocadlo, Earth and Plan. Sci. Lett. **254** 227 (2007).

[38] A. E. Petrova, V. N. Krasnorussky, and S. M. Stishov, J. of Exp. and Theor. Phys., **111**, 427. (2010).

[39] H. Asanuma, E. Ohtani, T. Sakai, H. Terasaki, S. Kamada, T. Kondo, T. Kikegawa, Phys. Chem. Minerals **37**, 353. (2010).

[40] J. Junquera et al., Phys. Rev. **B64**, 235111 (2001), J. M. Soler et al., J. Phys.: Condens. Matter **14**, 2745. (2002).

[41] Y. Dusansoy, J. Protas, R. Wandij, B. Roynes, Acta Cryst. **B27**, 1209 (1971).

[42] J. Tani, M. Takahashi, H. Kido, Intermet. **18** 1222 (2010).

[43] G. Malegori, L. Miglio, Phys. Rev. **B48**, 9223 (1993).

[44] H. Reuther, G. Behr and A. Teresiak, J. Phys.: Condens. Matter **13** L225. (2001).

[45] Y. Mori, H. Nakano, G. Sakane, G. Aquilanti, H. Udono, K. Takarabe, physica status solidi (b), **246**, 541. (2009).

[46] R. Caracas and R. Wentzcovitch, Geophys. Res. Lett., **31**, L20603 (2004).

[47] M. E. Schlesinger, Chem. Rev., **90**, 607. (1990).

[48] D. Santamaría-Pérez, R. Boehler, Earth and Plan. Sci. Lett. **265**, 743 (2008).

nd

TABLE VII: The summary of the basic results obtained for various polymorphs of FeSi using BOP-I. The DSFC method has been used for BOP+C.

polymorph	group	method	E_{cohes} (pw)	E_{cohes} (DFT)	a_{latt} (pw)	a_{latt} (DFT)	a_{latt} (EXP)
FeSi	(B1, NaCl)						
		BOP	-4.909	-5.181	4.410	4.95	
		BOP+C	-4.817		4.468		
FeSi	(B3, ZnS)						
		BOP	-4.593	-4.97	4.607	5.26	
		BOP+C	-4.312		4.659		
Fe_3Si	(Cu_3Au)						
		BOP		-5.99		3.595	
		BOP+C					
$FeSi_3$	($CuAu_3$)						
		BOP		-4.75		3.64	
		BOP+C					
α-$FeSi_2$	(tP3)						
		BOP		-5.2	a=2.685[a]	2.66[b]	2.69[b]
					c=5.072	5.08	5.134
		BOP+C					
					5.135		
β-$FeSi_2$	(oC48)						
		BOP	-4.376	-5.571	a=9.888	9.697[b]	9.865[c]
					b=7.904	7.759	7.791[c]
					c=7.811	7.839	7.833[c]
		BOP+C	-4.172	-5.571	9.957		
					7.959		
					7.865		
γ-$FeSi_2$	(C1, CaF_2)						
		BOP	-3.950		4.416		
		BOP+C	-3.950		4.416		
$FeSi_3$	($DO_3, AlFe_3$)	BOP-V	-4.129	-5.259	4.232	5.117	
		BOP+C	-4.080		4.244		
Fe_3Si	($DO_3, AlFe_3$)	BOP-V	-4.239		3.979		
		BOP+C	-3.885		4.294		

[a] 'pw' denotes present work, ref.[33], [b] present work obtained by SIESTA using relaxed cell calculation, [c] ref.[41], The net charges of $q = \pm 0.15$ were used for B1. DSFC: damped shift forced coulomb[20]. The long range cutoff distance $r_{cut} = 12.0$ Å.

[49] A. van de Walle and G. Ceder, Phys. Rev. **B59**, 14992 (1999).

[50] O. El-Atwani, S. Gonderman, A. DeMasi, A. Suslova, J. Fowler, M. El-Atwani, K. Ludwig, and J. P. Allain, J. Appl. Phys., **113**, 124305 (2013).

[51] Gaussian 03, Revision A.1, M. J. Frisch, G. W. Trucks, H. B. Schlegel, G. E. Scuseria, M. A. Robb, J. R. Cheeseman, J. A. Montgomery, Jr., T. Vreven, K. N. Kudin, J. C. Burant, J. M. Millam, S. S. Iyengar, J. Tomasi, V. Barone, B. Mennucci, M. Cossi, G. Scalmani, N. Rega, G. A. Petersson, H. Nakatsuji, M. Hada, M. Ehara, K. Toyota, R. Fukuda, J. Hasegawa, M. Ishida, T. Nakajima, Y. Honda, O. Kitao, H. Nakai, M. Klene, X. Li, J. E. Knox, H. P. Hratchian, J. B. Cross, C. Adamo, J. Jaramillo, R. Gomperts, R. E. Stratmann, O. Yazyev, A. J. Austin, R. Cammi, C. Pomelli, J. W. Ochterski, P. Y. Ayala, K. Morokuma, G. A. Voth, P. Salvador, J. J. Dannenberg, V. G. Zakrzewski, S. Dapprich, A. D. Daniels, M. C. Strain, O. Farkas, D. K. Malick, A. D. Rabuck, K. Raghavachari, J. B. Foresman, J. V. Ortiz, Q. Cui, A. G. Baboul, S. Clifford, J. Cioslowski, B. B. Stefanov, G. Liu, A. Liashenko, P. Piskorz, I. Komaromi, R. L. Martin, D. J. Fox, T. Keith, M. A. Al-Laham, C. Y. Peng, A. Nanayakkara, M. Challacombe, P. M. W. Gill, B. Johnson, W. Chen, M. W. Wong, C. Gonzalez, and J. A. Pople, Gaussian, Inc., Pittsburgh PA, 2003.

[52] S. R. Phillpot and S. B. Sinnott, Science **325**, 1634-1635 (2009).

TABLE VIII: The summary of elastic properties and bulk modulus (GPa) obtained for the B20, B2 and $\beta - FeSi_2$ polymorphs of FeSi.

	BOP	BOP+C	dft	exp
B20 (ε-FeSi)				
C11	363.3	363.3	488[a]	316.7[b]
C12	161.4	149.6	213	112.9
C44	89.5	83.4	125	125.2
B[c]	228.7	230.4	176.2	180.8
Y[d]	264.1	277.1	358.6	257.4
μ[e]	0.31		0.26	
B2 (CsCl)				
C11	414.1	318.4		
C12	186.9	239.0		
C44	101.1	166.5		
B[c]	262.6	265.5	223[f]	222[f]
Y[d]	297.9	113.445		
$\alpha - FeSi_2$ (oC48)				
C11		120.5		
C12		47.3		
C44		-23.8		
B[c]			172[f]	
$\beta - FeSi_2$ (oC48)				
C11	267.6	266.8	314.6[g]	264[h]
C12	60.3	133.4	95.8	177[h]
C22	187.2	381.7	355.8	78[h]
C23	43.8	138.2	89.4	
C33	185.2	252.2	362.5	
C44	53.3	109.5	126.4	
C55	38.7	36.3	127.0	
C66	38.8	32.0	142.0	
B[c]	129.4	177.9	172.5	206[h]
Y[d]	245.4	177.9	312.0	
μ[e]	0.184	0.333	0.199	

[a] ref.[37], [b] ref.[38], [c] $B = \frac{1}{3}(c_{11} + 2c_{12})$ for anisotropic cubic crystals. [f] ref.[33], [g] ref.[42], [h] ref.[43] For the Youngs's modulus and for the Posisson ratio the relations $Y = \left[(c_{11} + 2c_{12}) \frac{c_{11} - c_{12}}{c_{11} + c_{12}} \right]$ and $\mu = \frac{c_{12}}{c_{11} + c_{12}}$ have been used.